THE JOURNAL OF PHYSICAL CHEMISTRY C

Article

Cite This: J. Phys. Chem. C 2019, 123, 4329−4340

pubs.acs.org/JPCC

Helical Chains of Diatomic Molecules as a Model for Solid-State Optical Rotation

Published as part of The Journal of Physical Chemistry virtual special issue "Young Scientists".

Ty Balduf and Marco Caricato*

Department of Chemistry, University of Kansas, 1567 Irving Hill Road, Lawrence, Kansas 66045, United States

Supporting Information

ABSTRACT: Optical rotation (OR) measurements are a common method for distinguishing chiral compounds, but it is not well understood how intra- and intermolecular interactions affect this electronic property. Theoretical comparisons with solution-phase measurements are hampered by the difficulty of modeling solvent effects and the isotropic averaging of the experimental observable. Solid-state OR experiments/calculations could alleviate these difficulties, but experimental measurements are challenging and computational efforts have been limited due to a lack of existing procedures. We report calculated OR tensor values for a series of helices of diatomic molecules that may serve as a benchmark in the development of general-purpose electronic structure methods to compute the optical rotation of solids, in particular, molecular crystals. We find that the OR tensors for small helix clusters show poor agreement with values converged with respect to the helix size, regardless of unit cell size. The dependence of the converged OR on the dihedral angle of homonuclear helices is well described by the Kirkwood polarizability model, indicating that nearest-neighbor interactions are very important, albeit not the only relevant interactions. Basis set comparisons suggest that the aug-cc-pVDZ basis is sufficient to obtain qualitatively accurate results.

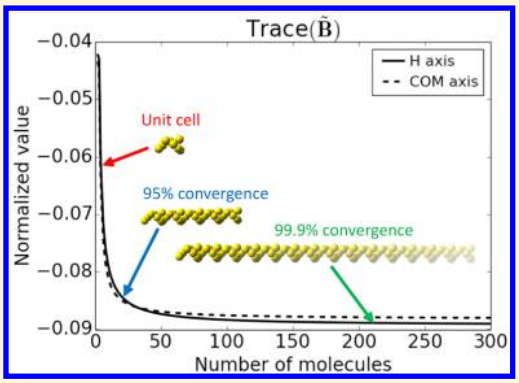

1. INTRODUCTION

Controlling supramolecular chirality is an active area of research with applications in nanostructure assembly,[1−3] drug design,[4] and enzymatic/bioinspired catalysis.[5,6] Optical activity measurements are commonly used to distinguish the chiral species generated in these experiments, but it remains poorly understood how the structure of a molecule and intermolecular interactions relate to the observed optical rotation (OR, referred to as *specific rotation* when it is normalized with respect to concentration and path length). Comparisons between computation and experiment could clarify this structure−property relationship, but such comparisons are hampered by limitations of existing theoretical methods. Most experimental measurements of optical activity are performed in solution, but theoretical methods to account for solvent effects are either highly costly or unable to account for specific solute−solvent interactions, making comparison with experiment challenging. Calculations of OR in isotropic media are also highly sensitive to cancellation effects: elements of the OR tensor can vary in sign and magnitude, so the calculated specific rotation, proportional to the trace of the OR tensor,[7,8] can be greatly influenced by small errors in OR tensor components. In experiment, one only obtains the isotropic specific rotation, not the OR tensor components, so comparison can show that a calculation is incorrect but not what is causing the error.

Some experimental work has sought to address these limitations by making measurements in different phases. Vaccaro et al. have used cavity ring-down polarimetry to study optical rotation in the gas phase.[9,10] Gas-phase measurements and calculations do not need to take into account intermolecular interactions, but they still need to deal with spatial averaging of the observable. Kahr and co-workers have enhanced techniques for isolating the OR of crystals from the typically much larger linear birefringence signal.[11−13] These solid-state measurements represent valuable benchmark data for theoretical comparison. While it is in principle possible to calculate the OR of solids and extended systems, one issue that remains is the development of a general computational procedure to do so. Perhaps due to the lack of experimental data available, neither classical nor first-principles techniques for calculating the OR of solids have been thoroughly pursued. To the best of our knowledge, the works of Zhong et al.,[14,15] using a combination of local density approximation density functional theory (DFT) and Green's functions, and Devarajan and Glazer,[16] utilizing the classical polarizability theory of optical rotation, have been the only attempts at developing such methods. However, both approaches rely on ad hoc

Received: December 16, 2018
Revised: January 19, 2019
Published: January 22, 2019

DOI: 10.1021/acs.jpcc.8b12084
J. Phys. Chem. C 2019, 123, 4329−4340

assumptions and parametrizations, thus lacking a truly general applicability.

In this work, we calculate the OR tensor of long helical chains of diatomic molecules (using the well-established procedure for isolated molecules) as a simple model for the behavior of extended systems. These calculations test the specifications, for example, cell size and basis set requirements, needed to accurately calculate the OR of infinite systems with the goal of using this information to develop and benchmark an efficient, general-purpose procedure to compute the optical activity of solids, in particular, molecular crystals.

The paper is organized as follows. In Section 2, we describe how the OR tensor is computed using the linear response formalism and our computational procedures. In Section 3, we present how the OR is influenced by the length and orientation of the helices, as well as the basis set used. We conclude the paper with a discussion of these results and their implications in Section 4.

2. THEORY

2.1. OR Tensor. Optical activity is governed by the rank-2 Buckingham/Dunn **B** tensor:[7,8]

$$B_{\alpha\beta} = \frac{1}{2}\left[\beta_{\alpha\beta} + \beta_{\beta\alpha} + \frac{1}{3}\sum_{\delta,\gamma}(\epsilon_{\alpha\gamma\delta}A_{\gamma,\delta\beta} + \epsilon_{\beta\gamma\delta}A_{\gamma,\delta\alpha})\right] \quad (1)$$

where, for nonrelativistic wave functions

$$\beta_{\alpha\beta} = 2\sum_{j\neq 0}\mathrm{Im}\frac{\langle\psi_0|\mu_\alpha|\psi_j\rangle\langle\psi_j|m_\beta|\psi_0\rangle}{\omega_j^2 - \omega^2} \quad (2)$$

$$A_{\alpha,\beta\gamma} = 2\sum_{j\neq 0}\omega_j\mathrm{Re}\frac{\langle\psi_0|\mu_\alpha|\psi_j\rangle\langle\psi_j|\Theta_{\beta\gamma}|\psi_0\rangle}{\omega_j^2 - \omega^2} \quad (3)$$

$\mu_\alpha = -\sum_i r_{i;\alpha}$ is the electric dipole operator, $m_\beta = -\sum_i \frac{1}{2}(\mathbf{r}\times\mathbf{p})_{i;\beta}$ is the magnetic dipole operator, and $\Theta_{\beta\gamma} = -\sum_i \frac{1}{2}(3r_\beta r_\gamma - \delta_{\beta\gamma}r^2)_i$ is the traceless electric quadrupole operator, with Greek indices denoting Cartesian coordinates; the sums in these operator definitions are over all of the electron coordinates of the molecule. ω is the frequency of the incident electromagnetic radiation, while $|\psi_j\rangle$ and ω_j are the jth excited state wave function and excitation frequency, respectively. These definitions are valid for nonresonant optical activity ($\omega_j \approx \omega$) calculations; resonant optical activity is discussed in greater detail elsewhere.[7,17,18]

$\boldsymbol{\beta}$ and **A** are, respectively, the frequency-dependent electric dipole−magnetic dipole and electric dipole−electric quadrupole polarizability tensors. Note that $\boldsymbol{\beta}$ is not to be confused with $-\omega\boldsymbol{\beta} = \mathbf{G}'$, which is also referred to as the electric dipole−magnetic dipole polarizability tensor and was used in the original formulation of the Buckingham/Dunn tensor.[7,8] While $\boldsymbol{\beta}$ and **A** are formally defined by eqs 2 and (3), direct application of these equations is impractical due to the large number of excited states needed to converge the OR tensor.[19] We instead compute the tensor via the linear response formalism, as detailed in Section 2.2.

The OR is commonly reported in terms of specific rotation (deg [dm (g/mL)]$^{-1}$) for isotropic media (e.g., gases and solutions), given by

$$\Delta\theta = -\frac{1}{3}\frac{\omega\mu_0}{m}(B_{xx} + B_{yy} + B_{zz}) = -\frac{1}{3}\frac{\omega\mu_0}{m}\mathrm{Tr}(\mathbf{B}) \quad (4)$$

where μ_0 is the permeability of free space, and m is the molecular mass. Contributions from **A** cancel out in this trace, so many prior studies[20−23] that focused on isotropic substances simply computed $\boldsymbol{\beta}$ to obtain the OR. For oriented materials (e.g., molecular crystals), individual Cartesian components of the OR tensor can be resolved experimentally, so it is important that we do not neglect the contributions from **A**. It is also convenient for calculations of oriented structures to reformulate **B** as

$$\tilde{B}_{\alpha\beta} = \frac{1}{2}[\mathrm{Tr}(\mathbf{B})\delta_{\alpha\beta} - B_{\alpha\beta}] \quad (5)$$

Letting **n** be a unit vector in some direction, the OR parameter $\beta_{\mathbf{n}}$, which is proportional to the specific rotation, is given as

$$\beta_{\mathbf{n}} = \mathbf{n}^\dagger\tilde{\mathbf{B}}\mathbf{n} \quad (6)$$

By defining this alternative chiroptical response tensor, one can easily compute the specific rotation for light traveling in an arbitrary direction relative to the oriented material.[8,17]

2.2. Linear Response Formalism. While it is formally possible to compute the OR tensor using the sum-over-states formulas of eqs 2 and (3), this approach requires prohibitively many excited states for the series to converge.[19] To circumvent this high cost, we instead compute the OR tensor using the linear response formalism.[24−26] This approach provides the same value of the property, but it casts the equations in terms of perturbations of the electron density due to an external oscillating field.[27] Adopting notation used by McWeeny[24] and Autschbach,[8] we can define the frequency-dependent polarizability $\boldsymbol{\Pi}(\mathbf{RS}|\omega)$ of a quantity **R** with respect to a perturbation **S** of frequency ω as

$$\Pi(\mathbf{RS}|\omega)_{\alpha\beta} = \begin{pmatrix}\mathbf{R}_\alpha\\ \mathbf{R}_\alpha^*\end{pmatrix}^\dagger\left[\begin{pmatrix}\mathbf{M} & \mathbf{Q}\\ \mathbf{Q}^* & \mathbf{M}^*\end{pmatrix} - \omega\begin{pmatrix}\mathbf{1} & \mathbf{0}\\ \mathbf{0} & -\mathbf{1}\end{pmatrix}\right]^{-1}\begin{pmatrix}\mathbf{S}_\beta\\ \mathbf{S}_\beta^*\end{pmatrix} = \begin{pmatrix}\mathbf{R}_\alpha\\ \mathbf{R}_\alpha^*\end{pmatrix}^\dagger\boldsymbol{\Omega}^{-1}\begin{pmatrix}\mathbf{S}_\beta\\ \mathbf{S}_\beta^*\end{pmatrix} \quad (7)$$

where, in Kohn−Sham DFT, $R_{\alpha,ai} = \langle a|R_\alpha|i\rangle$, $S_{\beta,ai} = \langle a|S_\beta|i\rangle$, $M_{ia,jb} = (\epsilon_a - \epsilon_i)\delta_{ij}\delta_{ab} + K_{aj,ib}$, and $Q_{ia,jb} = K_{ab,ij}$ with i, j denoting occupied orbitals and a, b denoting virtual orbitals. $K_{aj,ib} = \langle aj|\frac{1}{r-r'}|ib\rangle + \langle aj|f^{\mathrm{XC}}(r,r')|ib\rangle$ which gives the coupling due to Coulombic interactions and the exchange correlation kernel $f^{\mathrm{XC}}(r,r')$ of the functional.

To avoid explicitly forming $\boldsymbol{\Omega}^{-1}$, the perturbed density is evaluated by solving the linear system

$$\boldsymbol{\Omega}\begin{pmatrix}\mathbf{X}_\beta\\ \mathbf{Y}_\beta\end{pmatrix} = \begin{pmatrix}\mathbf{S}_\beta\\ \mathbf{S}_\beta^*\end{pmatrix} \quad (8)$$

This gives an amplitude vector that can be computed iteratively without the need to perform a costly (and often numerically unstable) matrix inversion, leading to faster calculations of the polarizability tensors.[28] To determine $\boldsymbol{\beta}$, we solve eq 8 with $S_\beta = \mu_\beta$ and insert the result into (7) with $R_\alpha = m_\alpha$, calculating the magnetic dipole induced by a time-dependent perturbing electric field (for variational methods, it would be equivalent to reverse the definitions of R_α and S_β and

DOI: 10.1021/acs.jpcc.8b12084
J. Phys. Chem. C 2019, 123, 4329−4340

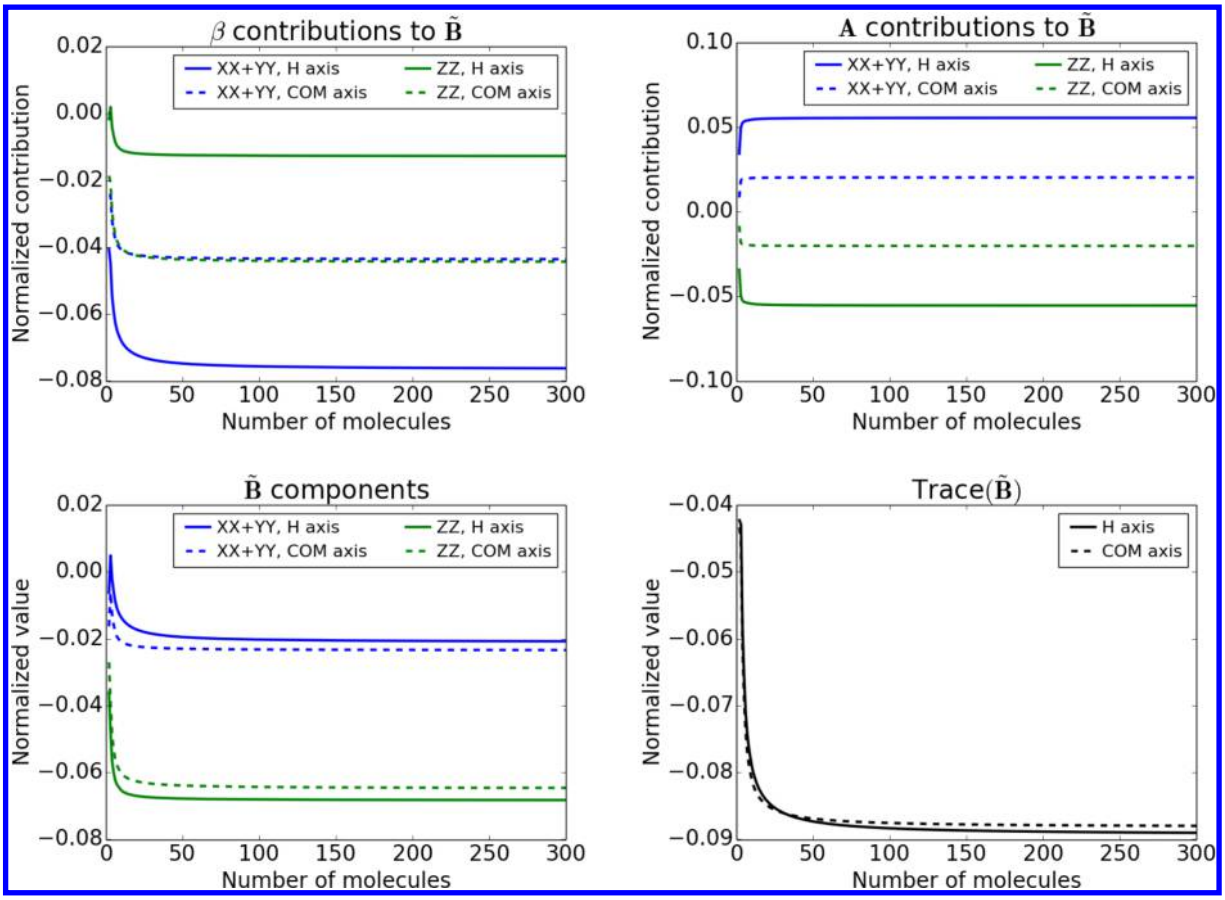

Figure 1. Plots of contributions to/components of $\tilde{\mathbf{B}}$ (a.u.) for a H_2 helix with 45° rotation about the COM and H atom axes. The separation between hydrogen molecules is 2.0 Å. Each value is scaled by the inverse of the number of units in the helix.

consider the electric dipole induced by a time-dependent magnetic field).[8] Similarly, to obtain **A**, the result of solving eq 8 with $S_\gamma = \mu_\gamma$ is inserted in eq 7 with $R_{\alpha\beta} = \Theta_{\alpha\beta}$, which gives the electric quadrupole induced by a time-dependent electric field.

2.3. Computational Procedure. In this paper, we consider helices formed from five diatomic molecules: H_2, N_2, F_2, HF, and LiH. Note that the optical activity in these model systems is solely generated by the supramolecular structure of the helices, as the individual molecular units are achiral. To generate the helices, we first orient a single diatomic molecule along the *y*-axis, with the origin centered either on one of its atoms (CA) or its center of mass (COM). We then add more units with coordinates determined by translating a distance *R* along the *z*-axis and rotating θ degrees counterclockwise in the *xy* plane. For each diatomic molecule, helices were generated with 15° increments up to 165°. Helices with 0° or 180° rotation have a plane of symmetry, and so they do not exhibit isotropic specific rotation; for these helices, this is not due to cancellation in the trace of the OR tensor, but rather from each diagonal component individually being zero. For this reason, we do not perform any further analysis of the OR tensor for these helix conformations. The distance *R* varies for the different molecules, with H_2 units separated by 2.0 Å; N_2, F_2, and HF units separated by 3.5 Å; and LiH units separated by 5.0 Å. These distances were chosen so that the molecular units would be close enough to retain significant intermolecular interactions while avoiding large electron density overlap between neighboring units. Experimental bond lengths from the NIST CCCBDB database[29] were used for each molecule: R_{H_2} = 0.741 Å, R_{N_2} = 1.098 Å, R_{F_2} = 1.412 Å, R_{HF} = 0.917 Å, R_{LiH} = 1.595 Å.

For each helix, the response to a 589.3 nm electromagnetic perturbation was computed using linear response as described in Section 2.2. All calculations were performed using a development version of the Gaussian suite of programs,[30] with the CAM-B3LYP functional[31] and aug-cc-pVDZ basis[32] in the length gauge representation, using gauge including atomic orbitals (GIAOs)[33] to ensure origin independence (origin independence could also be achieved using the modified-velocity gauge without GIAOs, but this leads to slower convergence of the OR with basis set size[25]). This choice of functional and basis set has been shown to accurately reproduce the OR obtained from experiment[8,34] and higher levels of theory.[35]

Since these helical systems cannot be experimentally realized nor have they been studied computationally, it is useful to have a model that can be related qualitatively to the calculated results. We compare these computed values with predictions based on the semiempirical Kirkwood polarizability model,[17,21,36,37] which expresses the optical rotation in terms of the mean polarizability and anisotropy of interacting groups. The model suggests that two interacting groups with $C_{nv}(n > 2)$ symmetry will contribute to the optical rotation in proportion to $\sin(2\theta)$, where θ is the dihedral angle between the groups.[17] This model can offer insight into the locality of interactions within the helices, since interactions beyond those

DOI: 10.1021/acs.jpcc.8b12084
J. Phys. Chem. C 2019, 123, 4329−4340

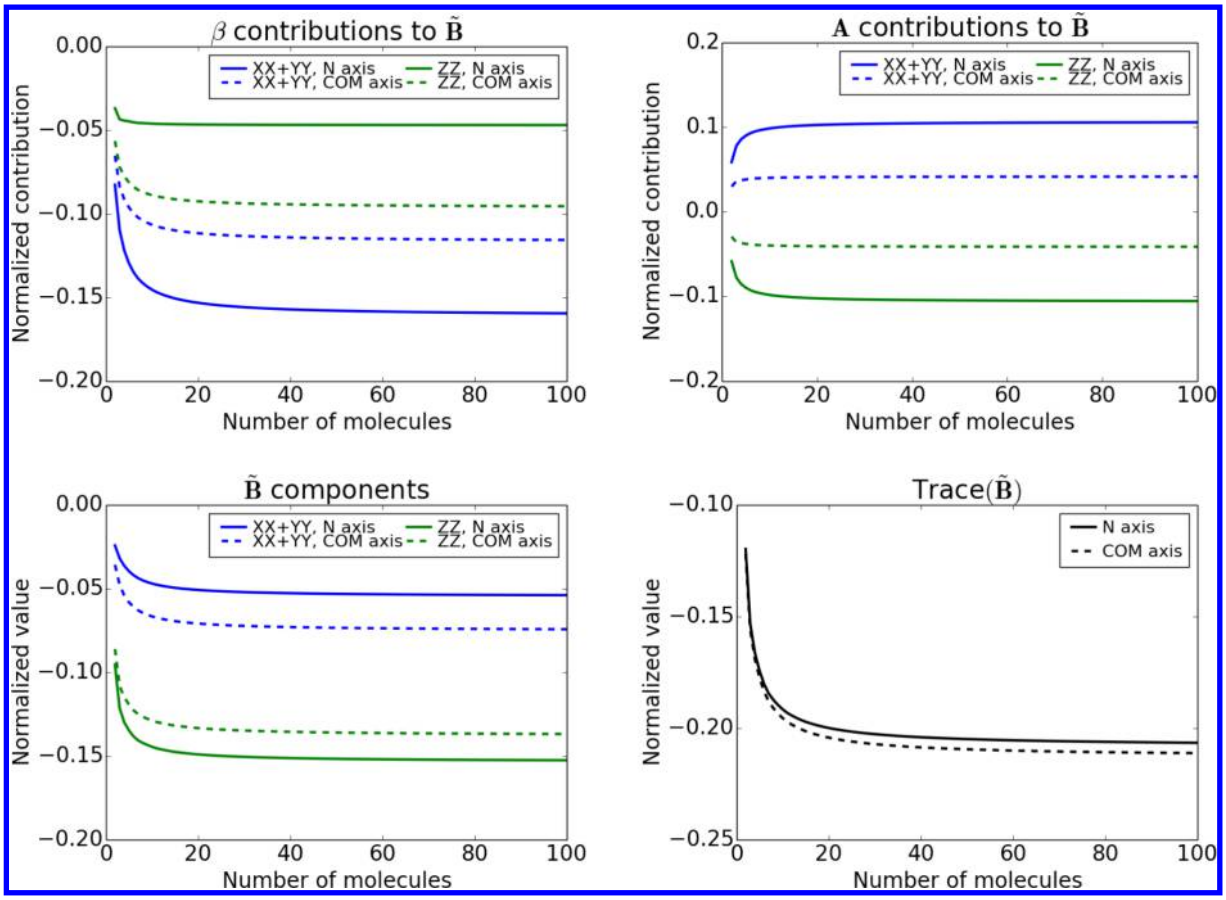

Figure 2. Plots of contributions to/components of $\tilde{\mathbf{B}}$ (a.u.) for a N_2 helix with 45° rotation about the COM axis and N atom axes. The separation between nitrogen molecules is 3.5 Å. Each value is scaled by the inverse of the number of units in the helix.

of nearest neighbors should introduce $\sin(2k\theta)$ contributions (k = 2,3,⋯).

3. RESULTS

To analyze the OR tensor, we plot the Cartesian components of $\tilde{\mathbf{B}}$, the contributions of $\boldsymbol{\beta}$ and $\mathbf{A}$ to these components, and $\mathrm{Tr}(\tilde{\mathbf{B}})$. All component contributions/values are scaled by the inverse of the number of units in the helix so that they can be directly related to the specific rotation. Since the helix is not periodic in the x or y direction, the XX and YY component contributions are combined to reflect the averaged value that would be observed in a hypothetical experimental measurement. We include plots of the trace of the OR tensor for completeness and clarity of certain comparisons; we emphasize that, for solid-state calculations, the specific rotation in each direction is given by eq 6, rather than the trace of $\tilde{\mathbf{B}}$, as there is no isotropic averaging.

In Section 3.1, we discuss the dependence of the OR tensor components (in particular, how quickly they converge) on the length of the helix considered. In Section 3.2, we discuss how the dihedral angle between each molecular unit influences the OR and utilize the Kirkwood model to probe interaction distances within the helices. In Section 3.3, we examine the basis set dependence of the results obtained for H_2.

3.1. Length Dependence. To model the calculation size necessary to converge the OR tensor components, we created helices of various lengths for each of the diatomic molecules. For H_2, we constructed all helices with up to 300 molecules for each dihedral angle and rotation axis considered, while for the other four molecules we obtained all lengths up to 100 molecules. We plot the diagonal Cartesian components of $\tilde{\mathbf{B}}$, as well as the contributions to these components from $\boldsymbol{\beta}$ and $\mathbf{A}$, with respect to the number of molecular units for representative helices with θ = 45° in Figures 1−4.

As expected based on the sum-over-states formula, the contribution of $\mathbf{A}$ to $\mathrm{Tr}(\tilde{\mathbf{B}})$ is zero (i.e., XX + YY = −ZZ), and this is the case for all the types of diatomic helices tested. However, the $\mathbf{A}$ tensor does influence the relative and absolute magnitude of the directional components of $\tilde{\mathbf{B}}$. For the COM helix described in Figure 1, had we assumed that $\boldsymbol{\beta}$ on its own represented the OR, the XX + YY and ZZ components would be predicted to have nearly equal magnitude, but with the contribution from $\mathbf{A}$ included, the ZZ component is actually ∼3 times larger than the XX + YY. For the H axis helix, $\mathbf{A}$ contributions essentially invert the ratio between the Cartesian components. These examples illustrate that including the electric dipole−electric quadrupole contribution is crucial to obtain the correct qualitative relationship between the Cartesian components of the OR tensor.

The homonuclear molecules exhibit remarkably similar variation of the OR tensor with respect to length, as can be seen by comparing Figures 1−3. This similarity holds across the whole range of dihedral angles, which implies that the qualitative OR behavior of these homonuclear systems is largely governed by the helix geometry rather than by the nature of the substituents. For H_2, the Cartesian components of $\tilde{\mathbf{B}}$ are typically 95% of their converged value within ∼25−35 molecules for all dihedral angles. For N_2, F_2, and HF, ∼20

DOI: 10.1021/acs.jpcc.8b12084
J. Phys. Chem. C 2019, 123, 4329−4340

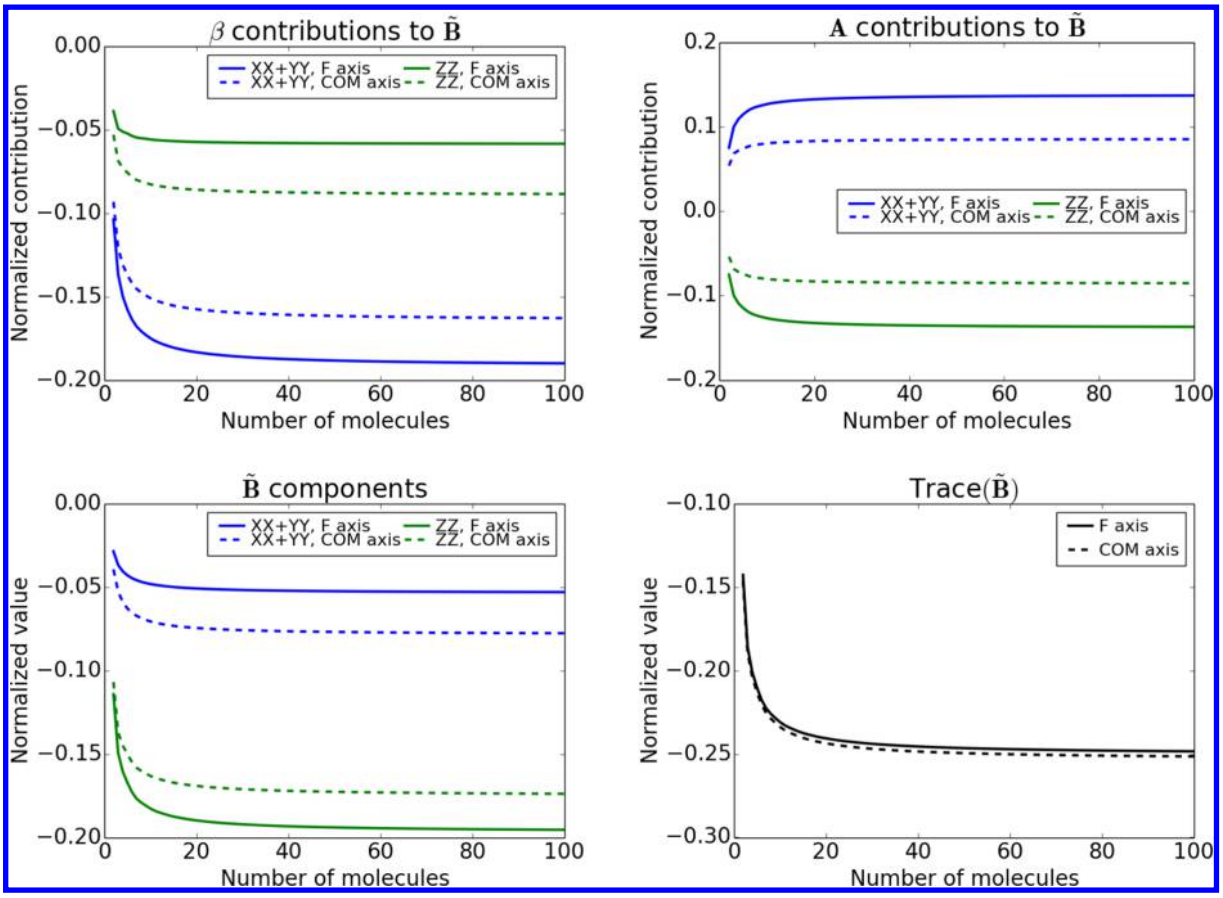

Figure 3. Plots of contributions to/components of $\tilde{\mathbf{B}}$ (a.u.) for a F_2 helix with 45° rotation about the COM and F atom axes. The separation between fluorine molecules is 3.5 Å. Each value is scaled by the inverse of the number of units in the helix.

molecules are needed to reach 95% of the converged value for every dihedral angle (LiH exhibited markedly different convergence behavior than the other molecules; thus, it will be treated separately below).

For small clusters (~2−7 molecules), the OR tensor components do not agree with their converged values. The OR components of the small helices vary inconsistently with increased length, unlike the monotonic convergence seen for larger helices, making it impossible to extrapolate to the large helix limit. In fact, the components for the small helices can even have the wrong sign compared to their converged values. Interestingly, this poor agreement for small helices, and the rate of convergence in general, seem to be independent of unit cell size. The latter depends on the intermolecular relative orientation, determined by the angle θ, and varies between 2(COM homonuclear)/3(CA or heteronuclear) molecular units for θ = 90° and 12(COM homonuclear)/24(CA or heteronuclear) molecular units for θ = 15°, 75°, 105°, 165°. One might have expected that helices with a smaller unit cell would have required fewer units to converge their OR tensors, as the structure is in some sense more complete for a given number of molecules. Furthermore, molecular crystals that are periodic in two or three dimensions will likely require many more molecules to converge the OR tensor than these simple models. On the basis of the deviation from the converged OR tensor values for these small helices, we expect that calculations on just the unit cell will not be sufficient to obtain accurate results. This indicates that calculations on finite clusters are likely not practical for more realistic systems, and periodic boundary conditions (PBC) may be necessary.[38,39]

Changing the separation distance between molecules does not qualitatively alter $\boldsymbol{\beta}$ and $\mathbf{A}$, but it does affect their relative contributions to $\tilde{\mathbf{B}}$, as shown in Figure 5 for H_2. These plots are for helices with the same dihedral angle as Figure 1 but with the separation distance between units increased from 2.0 to 3.0 Å (the latter plots only extend to helices 100 molecules in length, as the tensor components were sufficiently converged by this point). The $\boldsymbol{\beta}$ contribution to each component decreases in magnitude, while the $\mathbf{A}$ contributions increase in magnitude. Since the ZZ contribution from each tensor is negative, $\tilde{B}_{ZZ}$ remains negative and essentially of the same magnitude, but the XX + YY contributions have different signs, and the shift in magnitude causes this component of $\tilde{\mathbf{B}}$ to become positive. This again highlights the importance of the $\mathbf{A}$ tensor contributions: not only are the components of $\boldsymbol{\beta}$ and $\tilde{\mathbf{B}}$ qualitatively different for a given separation distance but they also do not respond in the same manner to a change in separation distance.

In the prior analysis, we did not discuss LiH helices; unlike the other molecules, the $\tilde{\mathbf{B}}$ tensor components for many of the LiH helices do not converge with the length of the helix, as shown in Figure 6 by the plots of the H axis rotated helix. The slow convergence of the OR tensor is particularly noticeable in the plot of $\mathrm{Tr}(\tilde{\mathbf{B}})$. Even considering helices of length up to 250 units, $\mathrm{Tr}(\tilde{\mathbf{B}})$ continues to change significantly when additional units are added. Changing the separation distance between LiH units from 5.0 to7.5 Å or 10.0 Å (reported in Figures S1

DOI: 10.1021/acs.jpcc.8b12084
J. Phys. Chem. C 2019, 123, 4329−4340

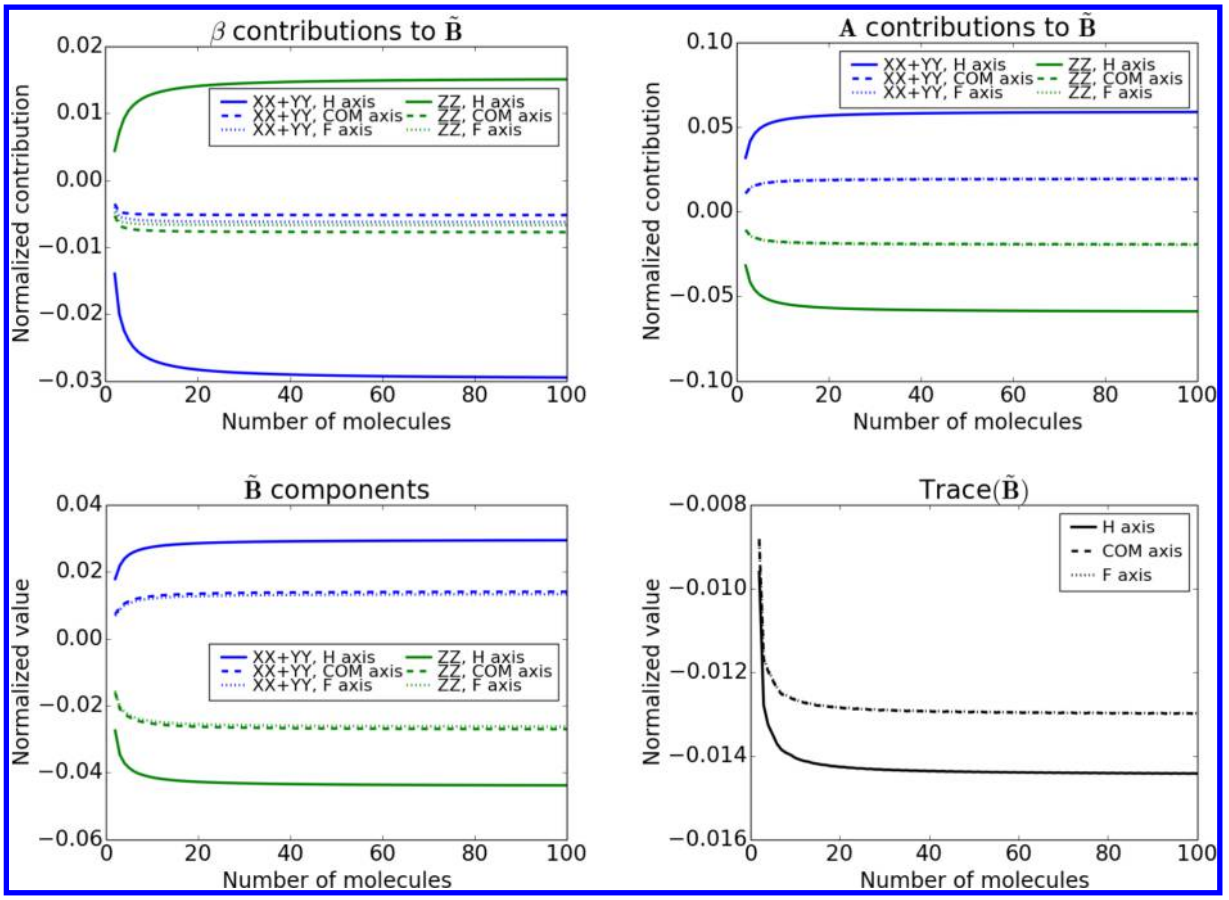

Figure 4. Plots of contributions to/components of $\tilde{\mathbf{B}}$ (a.u.) for a HF helix with 45° rotation about the COM, H atom, and F atom axes. The separation between HF molecules is 3.5 Å. Each value is scaled by the inverse of the number of units in the helix.

and S2 of the Supporting Information) did not make the $\mathrm{Tr}(\tilde{\mathbf{B}})$ curves smoother, although it did improve the rate of convergence for the 10.0 Å separation. That the error persists at different separation distances shows that it is not simply a consequence of the chosen geometry. Hartree−Fock calculations of the trace (see Figure S3 in the Supporting Information) seem to converge, albeit with oscillations about the converged value. To test whether the error is due to basis set incompleteness, Figure S4 in the Supporting Information reports $\mathrm{Tr}(\tilde{\mathbf{B}})$ calculated with the aug-cc-pVTZ basis, which shows that the OR tensor still fails to converge for some orientations and exhibits small oscillations throughout. These oscillations and jagged appearance of the $\mathrm{Tr}(\tilde{\mathbf{B}})$ curve occur in both DFT and Hartree−Fock calculations, suggesting they may be caused by edge effects from our finite model. Such edge effects may be present also in cluster models of realistic chiral crystals, further highlighting potential pitfalls of using finite models to describe solid crystals.

3.2. Angle Dependence. To study the influence of the helix geometry on the OR, we consider how the converged values of the OR tensor and its contributions vary as functions of the dihedral angle between units. In Figure 7, we plot the $\mathrm{Tr}(\tilde{\mathbf{B}})$ values for a series of H_2 helices with different dihedral angles θ for rotations around the COM and H atom axis. The plots for the individual components of the $\tilde{\mathbf{B}}$ tensor are reported for all molecules (but LiH) in Figures S5−S13 of the Supporting Information. The plots in Figure 7 seem to have a sinusoidal dependence on the angle that can be rationalized through the semiempirical Kirkwood polarizability model, as mentioned in Section 2.3.[21,37] Since the units of the helices have $D_{\infty h}$ or $C_{\infty v}$ symmetry depending on whether the molecule is homonuclear or heteronuclear, the Kirkwood model predicts interacting molecules will contribute to the optical rotation as $\sim\sin(2\theta')$ with respect to the angle θ' between them. For a given helix, $\theta' = k\theta$, $k = 1,2,\cdots$.

To see how well this model describes the results, we fit $\mathrm{Tr}(\tilde{\mathbf{B}})$ for each type of helix (excluding LiH, as its $\mathrm{Tr}(\tilde{\mathbf{B}})$ did not converge for many different dihedral angles and rotation axes) to the functional form $C\sin(\nu\theta)$, using a nonlinear regression, where C and ν are varied to minimize the sum of the mean-squared error with respect to the computed values. Figure 7 reports the fitted line for the H_2 helices (similar plots for N_2, F_2, and HF are given in Figures S14−S16 of the Supporting Information), while Tables 1 and 2 report the fitted C and ν parameters for all molecules. The fits for each axis are $\sim\sin(2\theta)$, which suggests that the largest contribution to the OR comes from nearest-neighbor interactions. Interestingly, the individual components of the $(\tilde{\mathbf{B}})$ tensor show a sinusoidal behavior only for helices with the COM axis, while for the helices with the axis on one of the atoms, only $\mathrm{Tr}(\tilde{\mathbf{B}})$ has a sinusoidal shape; see Figures S5−S13 in the Supporting Information.

Fitting the data a function of the form $C\sin(\nu\theta) + D\sin(\eta\theta)$ reduces the sum of the mean-square error by a factor of 2−4. These values are also reported in Tables 1−2 for all molecules (except LiH). For the homonuclear molecules, the refitting only marginally changes the values of C and ν (typically resulting in ν being closer to 2); D is anywhere from 4 to 10

DOI: 10.1021/acs.jpcc.8b12084
J. Phys. Chem. C 2019, 123, 4329−4340

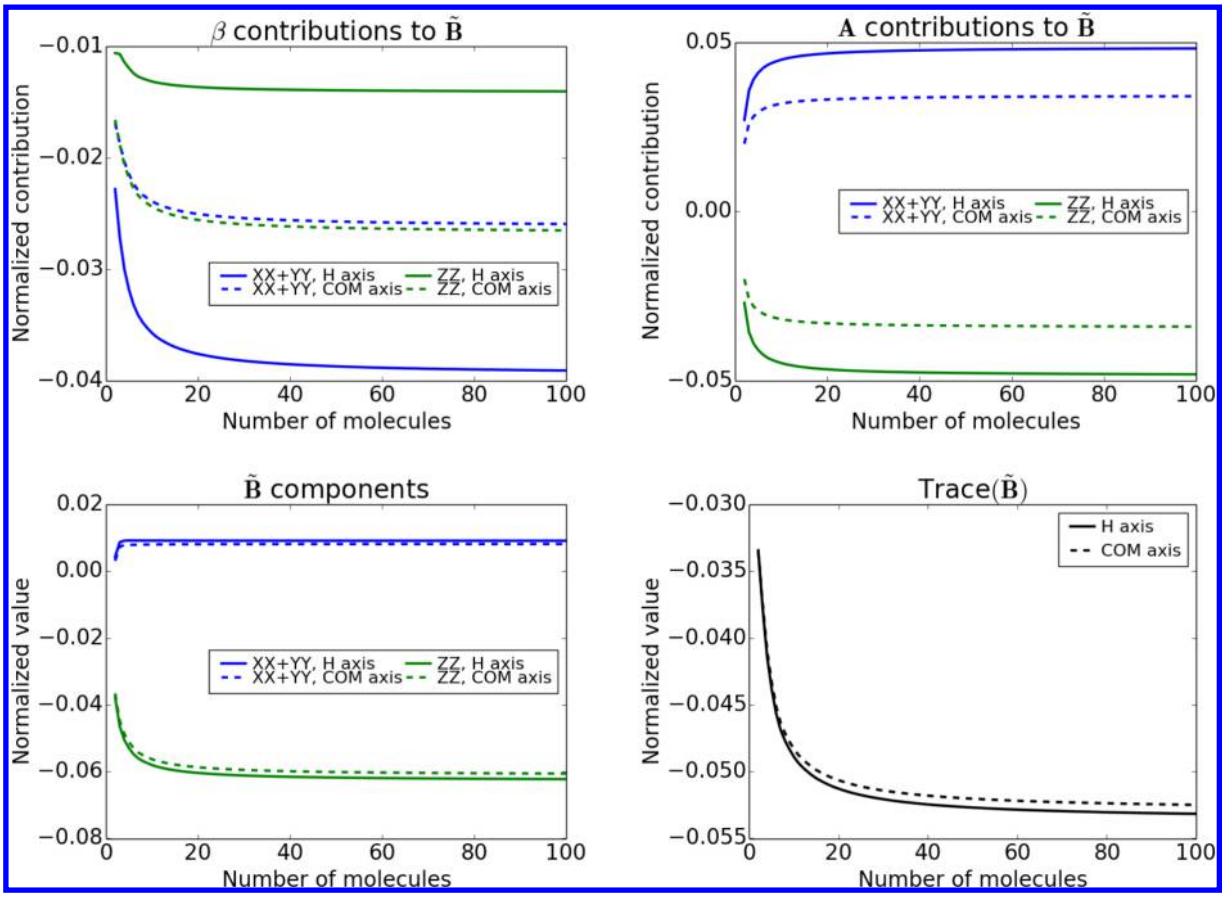

Figure 5. Plots of contributions to/components of $\tilde{\mathbf{B}}$ (a.u.) for a H_2 helix with 45° rotation about the COM axis. The separation between hydrogen molecules is 3.0 Å. Each value is scaled by the inverse of the number of units in the helix.

times smaller than C, and $\eta \approx 3.95$ for each molecule. These η and D values are consistent with the Kirkwood term arising from 2nd nearest-neighbor interactions, which we would expect to be the next largest contribution to the OR. For HF, while the error is reduced by the double sin fit, the ν and η parameters obtained for COM and F axis rotation clearly do not align with the Kirkwood model prediction. Different initial guesses for the HF double sin fit parameters did not decrease the mean squared error, nor did they significantly improve agreement with the Kirkwood model relative to the double sin fit in Tables 1 and 2. It is noteworthy that homonuclear H_2 and F_2 are described quite well with the Kirkwood model, but a heteronuclear combination of these elements generally does not agree with the model.

While the Kirkwood model provides a reasonable first-pass description of the OR, it is not a complete model even for homonuclear molecular units. In particular, angles close to 0° and 180° deviate from the fit, and the extrema of the fits (45° and 135°) do not match the extrema of the data (30° and 150°). While closer, the double sin fits' extrema also fail to match the data in the same regions. Since Kirkwood contributions all have the form $\sin(2k\theta)$, the model predicts that interacting groups rotated by 90° cannot contribute to the optical rotation; however, the atom axis helices for all molecules have a nonzero trace at 90°. Unlike rotation through the COM, 90° atom axis rotations leave the helix chiral; thus, $\mathrm{Tr}(\tilde{\mathbf{B}})$ can only be zero accidentally in this case. Moreover, a description of the OR in terms of solely local (kth nearest neighbor for small k) interactions would not be consistent with the results in Figures 1−4, as this would cause the OR tensor components to reach their converged values sooner. The fact that the OR tensor takes ∼25 units to converge suggests there must be some longer-range effects at play that are not properly described by the Kirkwood model and might be teased out from PBC calculations.

3.3. Basis Sets. The aug-cc-pVDZ basis set is generally a good compromise between computational cost and accuracy. However, in developing a solid-state OR procedure, it is important to verify that the conclusions we have drawn with this basis set are qualitatively consistent with the results of more complete basis sets. To this end, we compare aug-cc-pVDZ results for H_2 with calculations using aug-cc-pVTZ. In Figure 8, we plot the tensor contributions to/components of $\tilde{\mathbf{B}}$ using the aug-cc-pVTZ basis set, along with $\mathrm{Tr}(\tilde{\mathbf{B}})$ for the same H_2 helix as in Figure 1. Because of the cost associated with increasing the size of the basis set, results were only obtained for helices up to 100 molecules in length, which is sufficient to observe convergence of the tensor components. The tensor components obtained using the triple-ζ basis set exhibit similar qualitative behavior with respect to convergence as their double-ζ counterparts. The only noteworthy difference is that the $\tilde{\mathbf{B}}$ components shift to decrease their magnitude, leading to reduced optical response. This effect is essentially absent for the 90° helices, but it increases as θ goes toward 0° or 180°.

One exception to the qualitative similarity of the OR tensors in each basis set is the 15° helix, which shows an unusual stair-step pattern in the OR tensor and its trace; see Figure 9. These

DOI: 10.1021/acs.jpcc.8b12084
J. Phys. Chem. C 2019, 123, 4329−4340

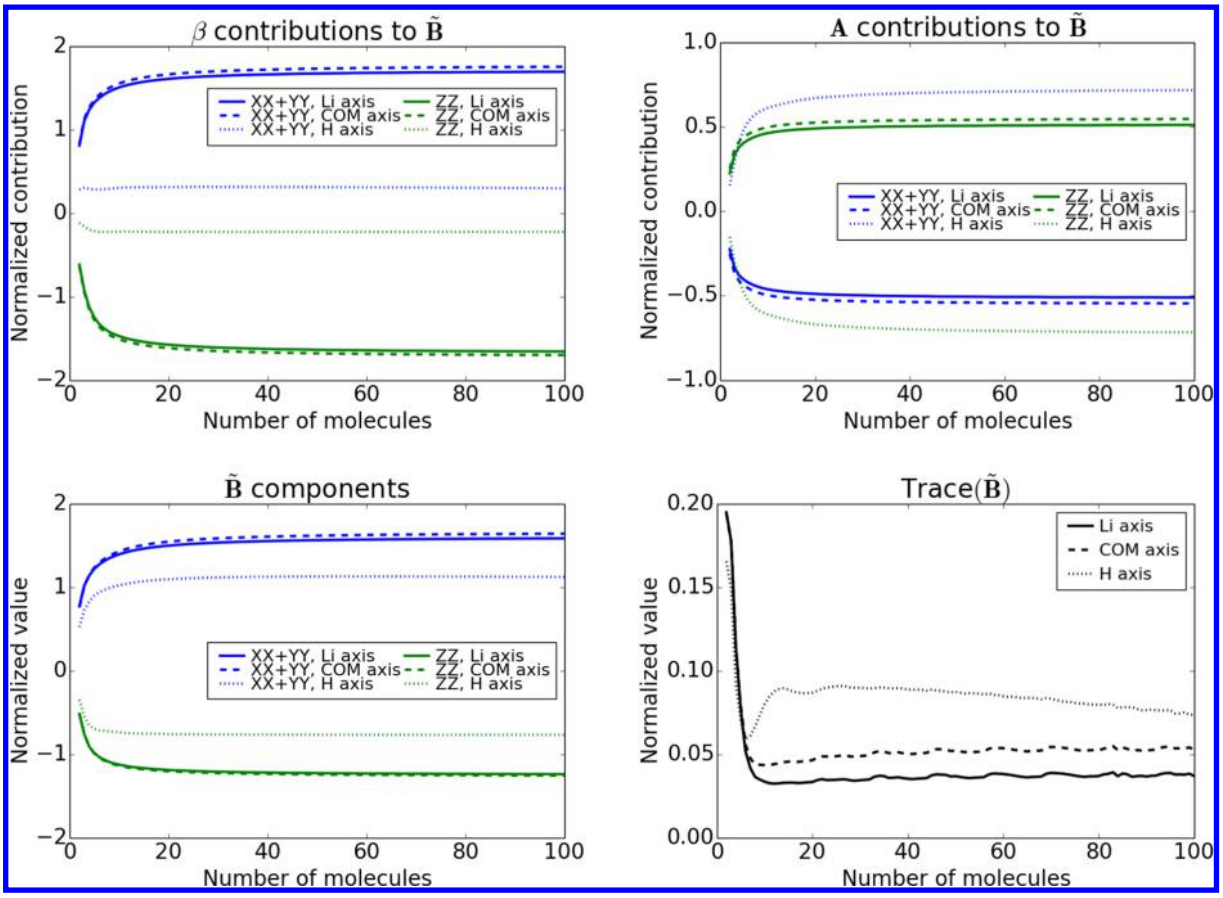

Figure 6. Plots of contributions to/components of $\tilde{\mathbf{B}}$ (a.u.) for a LiH helix with 30° rotation about the COM, Li atom, and H atom axes. The separation between LiH molecules is 5.0 Å. Each value is scaled by the inverse of the number of units in the helix.

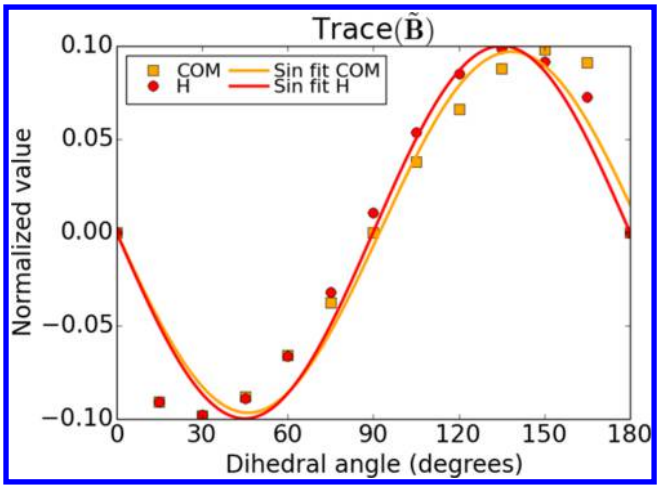

Figure 7. Converged Tr($\tilde{\mathbf{B}}$) (a.u.) for H_2 helices with θ° rotation about the H atom and COM axes. Points are the calculated values, and solid lines are single sin fits to the same colored calculated values. The separation between hydrogen molecules is 2.0 Å.

sharp jumps seem to be an unphysical artifact of the basis set, as evidenced by the incongruity between the periodicity of the steps and any geometric feature of the helix. To probe what part of the basis set causes this behavior, we repeated the calculations by systematically removing diffuse functions from the aug-cc-pVTZ basis. We focused on diffuse functions, because they have been shown to be more important for accurately computing the OR than other elements of the basis set.[23] On the one hand, we find that removing the s-type diffuse functions from the basis eliminates the sharp jumps and changes the values of the tensor components. On the other hand, removing d-type diffuse functions has little effect on the component values, while removing the p-functions substantially alters the OR tensor, leading to poor agreement with larger basis set results (vide infra).

To see whether this unphysical effect is present for larger bases and to test the accuracy of these diffuse-removed basis sets, we recalculated the OR using aug-cc-pVQZ and aug-cc-pV5Z, along with their variants, where some of the diffuse functions were removed. Figure 10 plots the trace of the OR tensor for a selection of these basis sets. We use the aug-cc-pV5Z results as the standard for accuracy, given that this is the largest basis set considered, although we note that p-pV5Z (the same basis set, but with only the p-type diffuse functions) gives very similar results. There are still jumps in $\tilde{\mathbf{B}}$ for the aug-cc-pVQZ basis; however, they do not occur in the same locations as they did for the aug-cc-pVTZ basis, supporting their unphysical nature. Comparing the fully augmented basis functions to those with just p-type diffuse functions, the results show that not only does removing the s-type functions smooth out the curves of Trace($\tilde{\mathbf{B}}$) but it also brings their values closer in line with those of the aug-cc-pV5Z basis set. This is a promising result, as it suggests that the accuracy of a large basis set can be achieved using a smaller cc-pVXZ basis with fewer diffuse functions.

DOI: 10.1021/acs.jpcc.8b12084
J. Phys. Chem. C 2019, 123, 4329−4340

Table 1. Fitting Parameters for Single and Double sin Fits of Tr($\tilde{\mathbf{B}}$) for COM Axis Rotations[a]

COM axis helices	single sin fit		double sin fit			
fitting parameters	$C \times 10^2$	ν	$C \times 10^2$	ν	$D \times 10^2$	η
H_2	−9.69	1.951	−9.81	1.992	−2.38	3.924
N_2	−21.9	1.980	−22.0	1.998	−2.35	3.943
F_2	−26.6	1.963	−26.8	1.996	−5.33	3.946
HF	−0.932	1.743	−0.935	1.346	−0.601	2.338

[a]Parameters were determined via nonlinear regression to minimize the sum of the mean-squared errors with respect to the calculated values of Tr($\tilde{\mathbf{B}}$) for each helix.

Table 2. Fitting Parameters for Single and Double sin Fits of Tr($\tilde{\mathbf{B}}$) for Atom Axis Rotations[a]

atom axis helices	single sin fit		double sin fit			
fitting parameters	$C \times 10^2$	ν	$C \times 10^2$	ν	$D \times 10^2$	η
H_2	−10.0	2.001	−10.3	2.034	−1.91	3.853
N_2	−17.9	1.946	−18.3	1.979	−2.67	3.706
F_2	−21.2	1.921	−21.8	1.979	−5.35	3.774
HF(H)	−1.45	1.885	−1.43	1.902	−0.296	4.140
HF(F)	−0.940	1.721	−0.932	1.341	−0.597	2.337

[a]Parameters were determined via nonlinear regression to minimize the sum of the mean-squared errors with respect to the calculated values of Tr($\tilde{\mathbf{B}}$) for each helix.

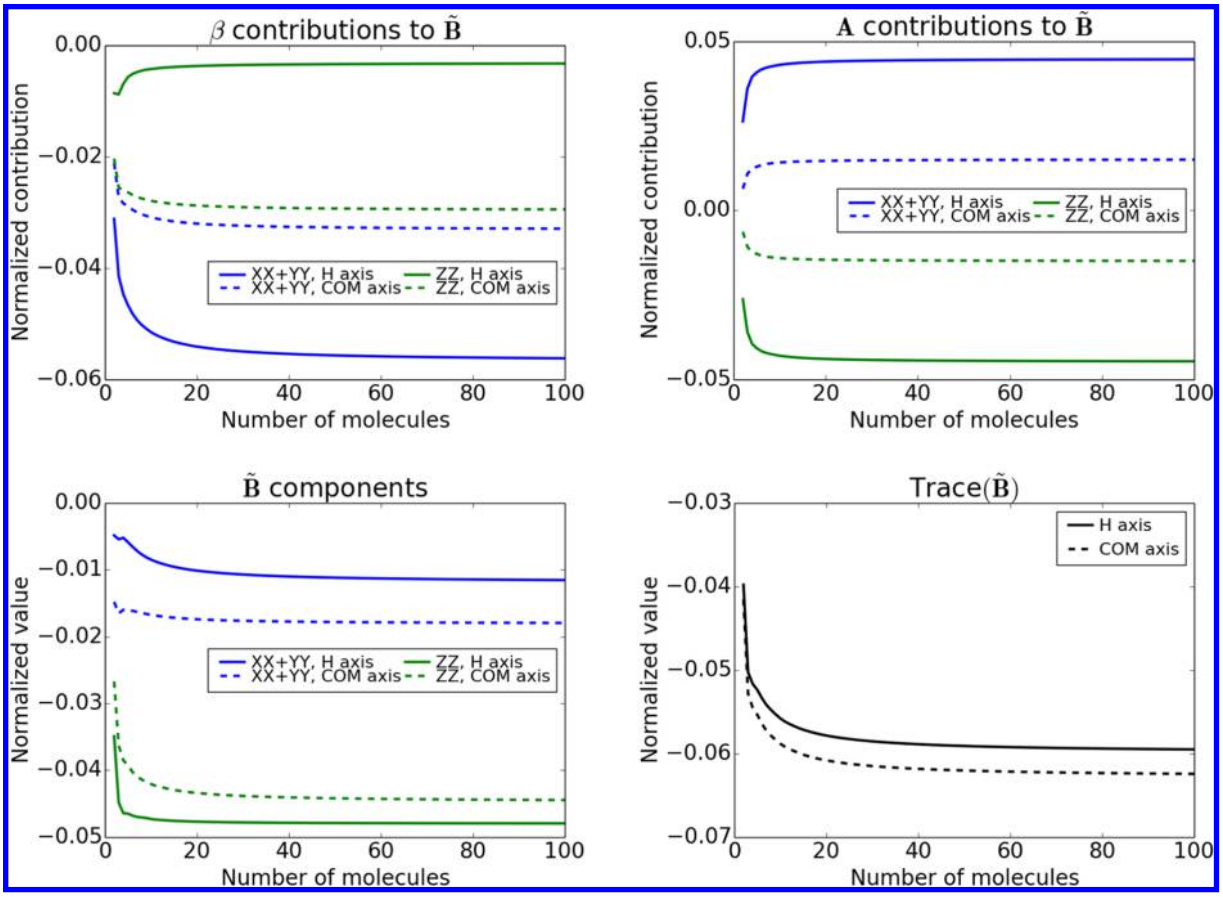

Figure 8. Plots of contributions to/components of $\tilde{\mathbf{B}}$ (a.u.) for a H_2 helix with 45° rotation about the H atom and COM axes. Calculations were performed using aug-cc-pVTZ basis set. The separation between hydrogen molecules is 2.0 Å. Each value is scaled by the inverse of the number of units in the helix.

4. DISCUSSION AND CONCLUSIONS

This work provides benchmark data on a set of helical chains of diatomic molecules as a first step toward developing a general purpose electronic structure method to compute the OR of solids. We study the rate and extent of convergence of the OR tensor, $\tilde{\mathbf{B}}$, with respect to the length of the helix, and we find that the values for unit cell sized clusters do not agree with the converged values for these helices. This lack of dependence on the unit cell size holds across different molecules and helix conformations, suggesting larger calcu-

DOI: 10.1021/acs.jpcc.8b12084
J. Phys. Chem. C 2019, 123, 4329−4340

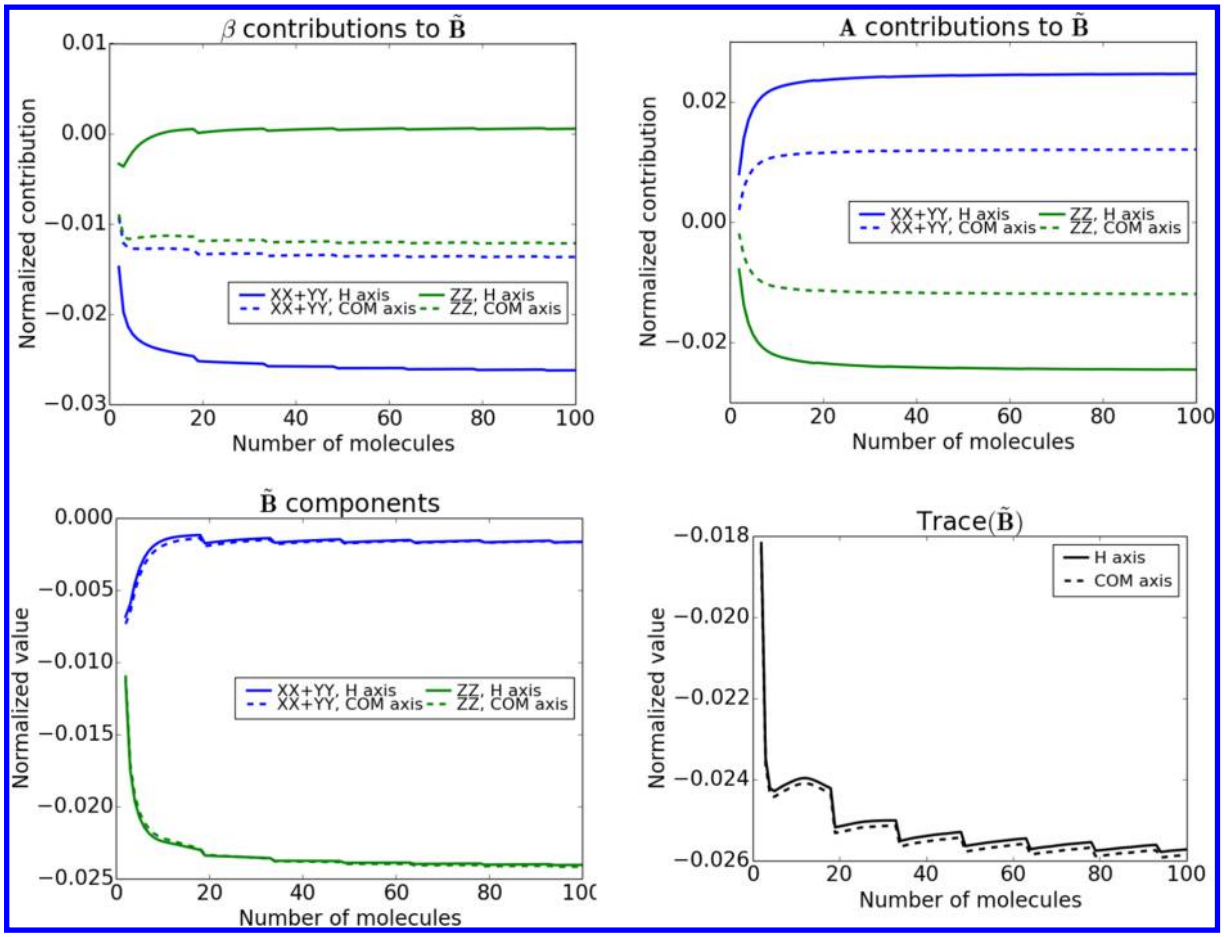

Figure 9. Plots of contributions to/components of $\tilde{\mathbf{B}}$ (a.u.) for a H_2 helix with 15° rotation about the H atom and COM axes. Calculations were performed using aug-cc-pVTZ basis set. The separation between hydrogen molecules is 2.0 Å. Each value is scaled by the inverse of the number of units in the helix.

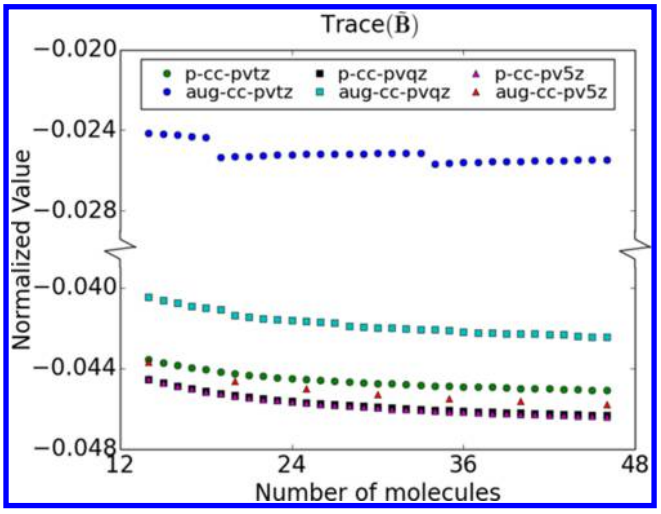

Figure 10. Plots of Trace($\tilde{\mathbf{B}}$) (a.u.) for a H_2 helix with 15° rotation about the COM axis. The separation between hydrogen molecules is 2.0 Å. Calculations were performed with the aug-cc-pVXZ basis sets, X = T,Q,5, and with the corresponding p-cc-pVXZ basis sets containing only p-type diffuse functions.

lation cells may be needed, particularly for the more relevant three-dimensional (3D) periodic compounds that we intend to study. The OR behavior of the helices of homonuclear molecular units with respect to the dihedral angle θ is in good agreement with the semiempirical Kirkwood polarizability model, indicating that nearest-neighbor interactions are the strongest contributions to the OR. At the same time, this simple model is not able to account for important long-range, cumulative interactions, and it does not describe heteronuclear helices very well. The difficulties of the Kirkwood model in describing even such simple systems reveal that approaches based on local polarizability may be insufficient to characterize chiral supramolecular assemblies. A comparison of the results for H_2 helices with different basis sets shows that the aug-cc-pVDZ results qualitatively agree with the results of the larger aug-cc-pVTZ basis set. Reasonable results are also obtained using basis sets with a reduced number of diffuse functions, allowing for more efficient computation of the OR.

The outcomes of this study suggest that the implementation of periodic boundary condition methods for the evaluation of the OR seems the best approach to study the optical activity of solids, and this work is currently underway in our group. Furthermore, the insight gained from these helix models will help us to tune various parameters of the PBC procedure to strike the right balance between accuracy and feasibility.

■ ASSOCIATED CONTENT

Ⓢ Supporting Information

The Supporting Information is available free of charge on the ACS Publications website at DOI: 10.1021/acs.jpcc.8b12084.

DOI: 10.1021/acs.jpcc.8b12084
J. Phys. Chem. C 2019, 123, 4329−4340

Plots of Tr($\tilde{\mathbf{B}}$) of LiH helices for alternate separations (7.5 Å, 10.0 Å), basis set (aug-cc-pVTZ), and level of theory (Hartree−Fock) of the 30° H-axis rotated LiH. Plots of the converged components of $\tilde{\mathbf{B}}$, along with the contributions of $\boldsymbol{\beta}$ and $\mathbf{A}$ to these components, for H_2, N_2, F_2, and HF with respect to dihedral angle along each rotation axis. Single sin fit curves of Tr($\tilde{\mathbf{B}}$) for N_2, F_2, and HF (PDF)

AUTHOR INFORMATION

Corresponding Author

*E-mail: mcaricato@ku.edu.

ORCID

Marco Caricato: 0000-0001-7830-0562

Notes

The authors declare no competing financial interest.

Biography

Marco Caricato earned his M.S. in Chemistry at the Università di Pisa (Italy) in 2003 and his Ph.D. in Chemistry at the Scuola Normale Superiore (Italy) in 2006 under the supervision of Jacopo Tomasi. From 2006 to 2010, he worked as postdoctoral researcher with Ken Wiberg at Yale University, and from 2010 to 2014 as research scientist at Gaussian, Inc. before becoming a professor at the University of Kansas in 2014. His research interests involve the development and application of quantum mechanical methods to condensed-phase systems for the investigation of reactivity and light−matter interactions.

ACKNOWLEDGMENTS

The authors gratefully acknowledge support from the National Science Foundation through Grant No. CHE-1650942.

REFERENCES

(1) Mastroianni, A. J.; Claridge, S. A.; Alivisatos, A. P. Pyramidal and chiral groupings of gold nanocrystals assembled using DNA scaffolds. *J. Am. Chem. Soc.* **2009**, *131*, 8455−8459.

(2) Chen, W.; Bian, A.; Agarwal, A.; Liu, L.; Shen, H.; Wang, L.; Xu, C.; Kotov, N. A. Nanoparticle superstructures made by polymerase chain reaction: Collective interactions of nanoparticles and a new principle for chiral materials. *Nano Lett.* **2009**, *9*, 2153−2159.

(3) Zhang, C.; Wu, W.; Li, X.; Tian, C.; Qian, H.; Wang, G.; Jiang, W.; Mao, C. Controlling the chirality of DNA nanocages. *Angew. Chem., Int. Ed.* **2012**, *51*, 7999−8002.

(4) Brooks, W. H.; Guida, W. C.; Daniel, K. G. The significance of chirality in drug design and development. *Curr. Top. Med. Chem.* **2011**, *11*, 760−770.

(5) Hu, L.; Ren, Y.; Ramström, O. Chirality control in enzyme-catalyzed dynamic kinetic resolution of 1,3-oxathiolanes. *J. Org. Chem.* **2015**, *80*, 8478−8481.

(6) Takata, S.; Endo, Y.; Shahid Ullah, M.; Itsuno, S. Synthesis of cinchona alkaloid sulfonamide polymers as sustainable catalysts for the enantioselective desymmetrization of cyclic anhydrides. *RSC Adv.* **2016**, *6*, 72300−72305.

(7) Buckingham, A. D.; Dunn, M. B. Optical activity of oriented molecules. *J. Chem. Soc. A* **1971**, 1988−1991.

(8) Autschbach, J. Time-dependent density functional theory for calculating origin-independent optical rotation and rotatory strength tensors. *ChemPhysChem* **2011**, *12*, 3224−3235.

(9) Müller, T.; Wiberg, K. B.; Vaccaro, P. H. Cavity ring-down polarimetry (CRDP): A new scheme for probing circular birefringence and circular dichroism in the gas phase. *J. Phys. Chem. A* **2000**, *104*, 5959−5968.

(10) Müller, T.; Wiberg, K. B.; Vaccaro, P. H.; Cheeseman, J. R.; Frisch, M. J. Cavity ring-down polarimetry (CRDP): theoretical and experimental characterization. *J. Opt. Soc. Am. B* **2002**, *19*, 125−141.

(11) Claborn, K.; Herreros Cedres, J.; Isborn, C.; Zozulya, A.; Weckert, E.; Kaminsky, W.; Kahr, B. Optical rotation of achiral pentaerythritol. *J. Am. Chem. Soc.* **2006**, *128*, 14746−14747.

(12) Kahr, B.; Freudenthal, J.; Gunn, E. Crystals in light. *Acc. Chem. Res.* **2010**, *43*, 684−692.

(13) Martin, A. T.; Nichols, S. M.; Li, S.; Tan, M.; Kahr, B. Double cone of eigendirections in optically active ethylenediammonium selenate crystals. *J. Appl. Crystallogr.* **2017**, *50*, 1117−1124.

(14) Zhong, H.; Levine, Z. H.; Allan, D. C.; Wilkins, J. W. Optical activity of selenium: A nearly first-principles calculation. *Phys. Rev. Lett.* **1992**, *69*, 379−382.

(15) Zhong, H.; Levine, Z. H.; Allan, D. C.; Wilkins, J. W. Band-theoretic calculations of the optical-activity tensor of α-quartz and trigonal Se. *Phys. Rev. B: Condens. Matter Mater. Phys.* **1993**, *48*, 1384−1403.

(16) Devarajan, V.; Glazer, A. Theory and computation of optical rotatory power in inorganic crystals. *Acta Crystallogr., Sect. A: Found. Crystallogr.* **1986**, *A42*, 560−569.

(17) Barron, L. D. *Molecular Light Scattering and Optical Activity,* 2nd ed.; Cambridge University Press: Cambridge, UK, 2004.

(18) Krykunov, M.; Autschbach, J. Calculation of origin-independent optical rotation tensor components in approximate time-dependent density functional theory. *J. Chem. Phys.* **2006**, *125*, 034102.

(19) Wiberg, K. B.; Wang, Y. G.; Wilson, S. M.; Vaccaro, P. H.; Cheeseman, J. R. Sum-over-states calculation of the specific rotations of some substituted oxiranes, chloropropionitrile, ethane, and norbornenone. *J. Phys. Chem. A* **2006**, *110*, 13995−14002.

(20) Crawford, T. D. Ab initio calculation of molecular chiroptical properties. *Theor. Chem. Acc.* **2006**, *115*, 227−245.

(21) Ruud, K.; Helgaker, T. Optical rotation studied by density-functional and coupled-cluster methods. *Chem. Phys. Lett.* **2002**, *352*, 533−539.

(22) Hedegård, E. D.; Jensen, F.; Kongsted, J. Basis set recommendations for DFT calculations of gas-phase optical rotation at different wavelengths. *J. Chem. Theory Comput.* **2012**, *8*, 4425−4433.

(23) Stephens, P. J.; Devlin, F. J.; Cheeseman, J. R.; Frisch, M. J. Calculation of optical rotation using density functional theory. *J. Phys. Chem. A* **2001**, *105*, 5356−5371.

(24) McWeeny, R. In *Methods of Molecular Quantum Mechanics,* 2nd ed.; Craig, D. P., McWeeny, R., Eds.; Academic Press: San Diego, CA, 1978.

(25) Autschbach, J.; Nitsch-Velasquez, L.; Rudolph, M. Time-dependent density functional response theory for electronic chiroptical properties of chiral molecules. *Top. Curr. Chem.* **2010**, *298*, 1−98.

(26) Krykunov, M.; Autschbach, J. Calculation of optical rotation with time-periodic magnetic-field-dependent basis functions in

DOI: 10.1021/acs.jpcc.8b12084
J. Phys. Chem. C 2019, 123, 4329−4340

approximate time-dependent density-functional theory. *J. Chem. Phys.* **2005**, *123*, 114103.
(27) Crawford, T. D.; Tam, M. C.; Abrams, M. L. The current state of ab initio calculations of optical rotation and electronic circular dichroism spectra. *J. Phys. Chem. A* **2007**, *111*, 12057−12068.
(28) Frisch, M.; Head-Gordon, M.; Pople, J. Direct analytic SCF second derivatives and electric field properties. *Chem. Phys.* **1990**, *141*, 189−196.
(29) Johnson, R. D., III, Ed. *NIST Computational Chemistry Comparison and Benchmark Database, NIST Standard Reference Database Number 101, Release 19*. http://cccbdb.nist.gov/, accessed July 25, 2018. DOI: 10.18434/T47C7Z.
(30) Frisch, M. J.; Trucks, G. W.; Schlegel, H. B.; Scuseria, G. E.; Robb, M. A.; Cheeseman, J. R.; Scalmani, G.; Barone, V.; Petersson, G. A.; Nakatsuji, H.; et al. *Gaussian Development Version Revision I.11;* Gaussian, Inc., 2016.
(31) Yanai, T.; Tew, D. P.; Handy, N. C. A new hybrid exchange-correlation functional using the Coulomb-attenuating method (CAM-B3LYP). *Chem. Phys. Lett.* **2004**, *393*, 51−57.
(32) Dunning, T. H. Gaussian basis sets for use in correlated molecular calculations. I. The atoms boron through neon and hydrogen. *J. Chem. Phys.* **1989**, *90*, 1007.
(33) Ditchfield, R. Self-consistent perturbation theory of diamagnetism I. A gauge-invariant LCAO method for NMR chemical shifts. *Mol. Phys.* **1974**, *27*, 789−807.
(34) Stephens, P. J.; McCann, D. M.; Cheeseman, J. R.; Frisch, M. J. Determination of absolute configurations of chiral molecules using ab initio time-dependent density functional theory calculations of optical rotation: How reliable are absolute configurations obtained for molecules with small rotations? *Chirality* **2005**, *17*, S52−S64.
(35) Jorge, F. E.; De Oliveira, A. Z.; Silva, T. P. CAM-B3LYP optical rotations at different wavelengths: Comparison with CCSD results. *Int. J. Quantum Chem.* **2016**, *116*, 21−26.
(36) Polavarapu, P.; Chakraborty, D.; Ruud, K. Molecular optical rotation: An evaluation of semiempirical models. *Chem. Phys. Lett.* **2000**, *319*, 595−600.
(37) Kirkwood, J. G. On the theory of optical rotatory power. *J. Chem. Phys.* **1937**, *5*, 479.
(38) Kudin, K. N.; Scuseria, G. E. Linear-scaling density-functional theory with Gaussian orbitals and periodic boundary conditions: Efficient evaluation of energy and forces via the fast multipole method. *Phys. Rev. B: Condens. Matter Mater. Phys.* **2000**, *61*, 16440−16453.
(39) Izmaylov, A. F.; Brothers, E. N.; Scuseria, G. E. Linear-scaling calculation of static and dynamic polarizabilities in Hartree-Fock and density functional theory for periodic systems. *J. Chem. Phys.* **2006**, *125*, 224105.

DOI: 10.1021/acs.jpcc.8b12084
J. Phys. Chem. C 2019, 123, 4329−4340